The Astrophysical Journal, 953:20 (10pp), 2023 August 10 https://doi.org/10.3847/1538-4357/acdc21

The First Instrumentally Documented Fall of an Iron Meteorite: Orbit and Possible Origin

Ihor Kyrylenko[1], Oleksiy Golubov[1,2], Ivan Slyusarev[1], Jaakko Visuri[3], Maria Gritsevich[3,4,5], Yurij N. Krugly[1,2], Irina Belskaya[1,6], and Vasilij G. Shevchenko[1]
[1] Institute of Astronomy of V.N. Karazin Kharkiv National University, 35 Sumska Street, Kharkiv 61022, Ukraine; ihor.kyrylenko@karazin.ua
[2] Astronomical Observatory Institute, Faculty of Physics, A. Mickiewicz University, Poznan, Poland
[3] Finnish Fireball Network, Ursa Astronomical Association, Kopernikuksentie 1, Helsinki FI-00130, Finland
[4] Finnish Geospatial Research Institute, Vuorimiehentie 5, FI-02150 Espoo, Finland
[5] Department of Physics, University of Helsinki, Gustaf Hällsrömin katu 2a, Helsinki FI-00014, Finland
[6] LESIA, Observatoire de Paris, Université PSL, CNRS, Université Paris Cité, Sorbonne Université, Meudon, France
Received 2023 February 2; revised 2023 May 26; accepted 2023 June 5; published 2023 July 28

Abstract

A bright fireball observed on 2020 November 7, over Scandinavia, produced the first iron meteorite with a well-determined pre-atmospheric trajectory. We calculated the orbit of this meteoroid and found that it demonstrates no close affinity with the orbit of any known asteroid. We found that the meteoroid (or its parent body) most probably entered the near-Earth orbit from the main asteroid belt via either ν_6 secular resonance with Saturn (89%) or 3:1 mean-motion resonance with Jupiter (11%). The long YORP timescale of the meteoroid suggests that it could have been produced in the main asteroid belt and survived the journey to the near-Earth orbit.

Unified Astronomy Thesaurus concepts: Iron meteorites (863); Meteorites (1038); Meteoroids (1040); Meteors (1041); Fireballs (538); Asteroids (72); Celestial mechanics (211); Astronomical simulations (1857)

1. Introduction

Among >71,500 officially classified meteorites, only a small fraction (about 2%) are of iron composition.[7] Iron meteorites are thought to be fragments of molten metallic cores or pools that formed in differentiated and subsequently disrupted planetesimals. The processes related to the formation of the iron meteorite parent bodies could be revealed by the thermal history of their crystallization and cosmic-ray exposure ages (CRE) (Goldstein et al. 2009; Kaminski et al. 2020; Scott 2020).

Chemical and isotopic analysis of iron meteorites allows us to divide them into 14 groups, presumably originating in different planetesimals. The four largest groups contain 75% of all iron meteorites, whereas about 15% of ungrouped irons appear to come from at least 50 other parent bodies (Burbine et al. 2002). This makes iron meteorites one of the most diverse groups of meteorites. Nevertheless, the location and size of the parent bodies of iron meteorites and their subsequent dynamical evolution remain a matter of debate (Bottke et al. 2006).

Finding a relationship between different populations of small bodies has always advanced our understanding of their evolutionary paths. In the middle of the nineteenth century, some active meteor streams were associated with comets (Schiaparelli 1867). In 1983, it was found that the newly discovered asteroid 1983 TB, now known as (3200) Phaethon, has an orbit very similar to the Geminid meteoroid stream (Whipple 1983). Another well-known pairing is between the Quadrantid meteor shower and the near-Earth asteroid 2003 EH1 (Jenniskens 2004). Finally, parent asteroids were proposed for several meteorites with known orbits, e.g., Chelyabinsk, 2011 EO40 or (86039) 1999 NC43 (Borovička et al. 2013; de La Fuente Marcos & de La Fuente Marcos 2014); Annama, PHA 2014 UR116 (Trigo-Rodríguez et al. 2015); and Cavezzo, 2013 VC10 (Gardiol et al. 2021).

Up to now, only 46 meteorites have a sufficient set of video- or photodetection data on their atmospheric trajectory, allowing a reliable reconstruction of their heliocentric orbits before their entry into the Earth's atmosphere. Table 1 in Colas et al. (2020) provides a list of references to 38 meteorites with orbits derived from the records, which were acquired by the dedicated fireball networks or by other observational means. In addition to this data, several meteorites with known orbits have been recovered more recently, including Traspena (Andrade et al. 2022), Winchcombe (King et al. 2022), Antonin (Shrbený et al. 2022), Saint-Pierre-le-Viger (Meteoritical Bulletin, 112, 2023, in preparation) and Ådalen (this work).

During the early era of visual observations, the fall of six iron meteorites was witnessed and the character of their heliocentric orbits was estimated (Pickering 1910). Later, this work was continued by Astapovich (1939), but the data were insufficient to reliably determine the orbits. The orbit of a large meteoroid that produced the Sikhote-Alin meteorite shower in 1947 was estimated by Fesenkov (1951) based on a survey of eyewitnesses. In the last 40 yr, there have been several falls of iron meteorites, including Sokoto (2008, Nigeria), Kavarpura (2006, India), Ban Rhong Du (1993, Thailand), and Sterlitamak (1990, USSR), the latter weighing 325 kg and being the largest iron meteorite mass collected after the Sikhote-Alin so far. In total, the falls of 49 iron meteorites have been confirmed.

The lack of precisely determined orbits of iron meteoroids has long hindered the location of the source of iron meteorites in the main asteroid belt. Fortunately, the situation changed when a

[7] Meteoritical Bulletin Database, accessed on 2023 May 21, https://www.lpi.usra.edu/meteor/.

bright fireball was detected over Sweden from several Scandinavian countries on 2020 November 7, at 21:27:04 UTC.[8] A 13.8 kg meteorite fragment has been recovered near the village of Ådalen, Sweden. Although its detailed chemical and isotopic analysis has still not been conducted because of the meteorite ownership disputes, its metallic composition is doubtless (Gritsevich et al. 2021; Moilanen & Gritsevich 2021, 2022). Multiple observations of the fireball from Denmark, Finland, and Norway allowed its trajectory to be determined, which puts the meteoroid on an Apollo-type near-Earth orbit (Moilanen & Gritsevich 2021). Sonic signals were also detected on five stations of the International Monitoring System of the Comprehensive Nuclear-Test-Ban Treaty Organization and were reported on JPL Fireball and Bolide Data[9] as a 0.33 kt event recorded by the US Government Sensors.

This event gives us a unique opportunity to study the delivery mechanism of iron meteorites and to look for iron-rich reservoirs in the solar system. This paper presents our results of the reconstruction of the meteoroid's orbit, a search of its possible parent body among near-Earth asteroids, and an investigation of the meteoroid's delivery from the main asteroid belt to its near-Earth orbit.

2. Methods and Results

2.1. Orbital Elements of the Meteoroid

Since the sky above the cameras of the fireball network in Sweden was covered by clouds, the detailed instrumental records of the fireball were obtained by the Finnish Fireball Network (J. Moilanen J. et al. 2023, in preparation) and by the Norwegian meteor camera network (Fig. 1).[10] The fireball was seen over a large distance, at least as far as 720 km away (Moilanen & Gritsevich 2021). The initial data analysis was done by Esko Lyytinen in the following days after the event using the methods described in Lyytinen & Gritsevich (2013, 2016a) with account for the real atmospheric conditions (Lyytinen & Gritsevich 2016b). Using these data, the dark flight Monte Carlo (DFMC, Moilanen et al. 2021) simulation was made by Jarmo Moilanen to determine the location of possible meteorites on the ground. The analysis of the atmospheric trajectory has identified the case as a certain meteorite dropper, based on both the DFMC application and the α–β criterion (Gritsevich et al. 2012; Sansom et al. 2019; Moreno-Ibáñez et al. 2020; Peña-Asensio et al. 2021; Boaca et al. 2022; Peña-Asensio et al 2023). The low value of the mass loss parameter β of only ~0.5, obtained as described in Gritsevich (2009), also suggested the iron composition of the object.

To estimate the precision of the derived orbit, we have repeated the retrieval of the trajectory and orbit calculation/deviation using the FireOwl recent data-processing software of the Finnish Fireball Network (Visuri & Gritsevich 2021) (Table 1). To ensure the robustness of the result, the orbit was also reconstructed using already established Meteor Toolkit software (Dmitriev et al. 2015, 2018; Gritsevich et al. 2017). To estimate the uncertainties, we computed all of the possible combinations that produce the largest errors to the orbital solution. The errors are defined by several factors, such as the angular resolution of the camera, the angular resolution of the calibration, the measured pixel coordinates of the fireball, and the error in velocity. The resulting orbital elements and their uncertainties are shown in Table 2.

Although the derived orbital elements are only sensitive to the reconstructed orientation and the velocity of the fireball's trajectory, the scarcity of the available observational data limits the achievable accuracy of the orbital elements of the meteoroid. The longitude of the ascending node is the orbital element determined with the highest accuracy because its value naturally follows from the position the Earth had in its orbit at the instant of the collision with the meteoroid. The other orbital elements are determined at a lower relative accuracy, but are still sufficient to estimate their past evolution in a statistical sense.

2.2. Past Close Approaches to the Earth

Since the meteoroid's orbit intersects the orbit of the Earth, it is natural to expect that it could have had close near-Earth passages in the recent past. To characterize these passages, we compute the minimal intersection distance between the closest approaches of the meteoroid to the Earth. For backward numerical integrations of the orbits, we used GENGA package, which is an open-source hybrid symplectic *N*-body integrator (Grimm & Stadel 2014). GENGA code utilizes CUDA technology, which allows the use of GPUs for the numerical integration of a large number of bodies. Its code uses mixed variable integration with a direct *N*-body Bulirsch-Stoer method in case of close encounters. The resulting encounter distance of the meteoroid's clones shows that the meteoroid possibly had close encounters with the Earth throughout its orbital evolution (Figure 2). The sensitivity of the meteoroid's evolution to the gravitational perturbation during each Earth's encounter leads to stretching of the uncertainty ellipsoid of its orbital parameters. Thus, the orbit in the distant past cannot be predicted precisely and only statistical conclusions can be made about the probability of different past orbits.

2.3. Search for a Possible Parent Body of the Meteoroid by the Orbital Integration

We started our search for parent body candidates with the assumption that the meteoroid split from another near-Earth asteroid in the near past, thus their orbits may preserve resemblance in terms of their orbital elements. The meteoroid still could have been influenced by perturbations from the Earth during close passages because they were definitely possible (see Figure 3). If an orbit is principally perturbed by only one planet, then the orbital elements change but their combination called the Tisserand parameter remains quasi-constant. This feature allows the possibility of keeping track of objects with a similar value of the Tisserand parameter and comparing instantaneous orbits, whose origin could have been compromised by the perturbing forces.

The Tisserand parameter is defined as (e.g., Murray & Dermott 1999):

$$T_{\rm E} = \frac{a_{\rm E}}{a} + 2\cos i\sqrt{\frac{a}{a_{\rm E}}(1-e^2)}. \quad (1)$$

Here, a, e, and i are the semimajor axis, eccentricity, and inclination of the asteroid's orbit, $a_{\rm E}$ is the semimajor axis of the Earth's orbit, and $T_{\rm E}$ is the Tisserand parameter with respect to the Earth.

[8] International Meteor Organization, https://fireballs.imo.net/members/imo_view/event/2020/6403.
[9] Jet Propulsion Laboratory, Fireball and Bolide Data, https://cneos.jpl.nasa.gov/fireballs/.
[10] Norsk Meteornettverk, Enköpings kommun 2020 November 7 21:27:00 UTC, http://norskmeteornettverk.no/meteor/20201107/212700/.

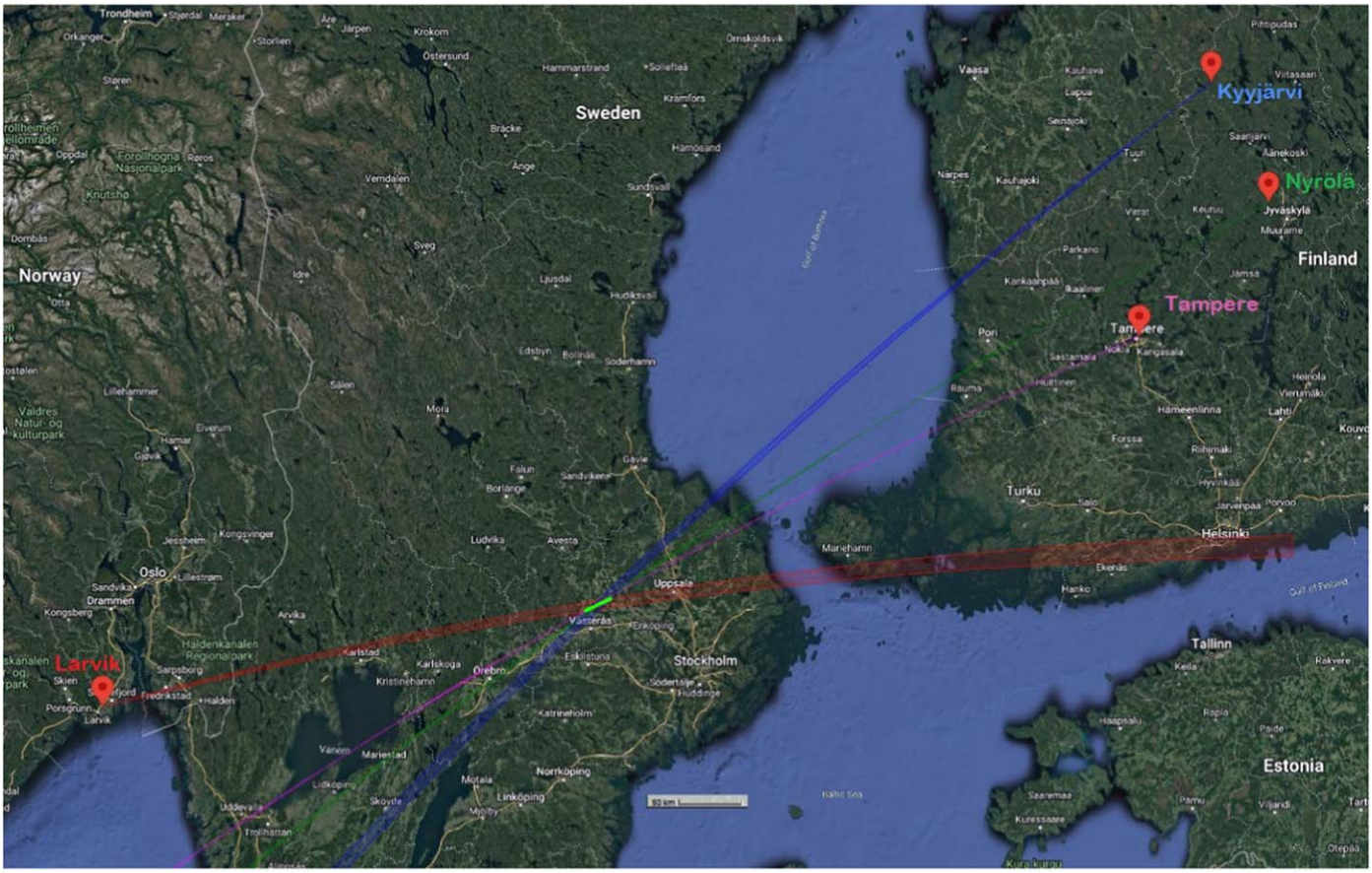

Figure 1. Triangulated trajectory of the fireball. The iron meteoroid came from the southwest and was heading in the northeast direction with a trajectory slope of over 73°. Of all the stations, only four stations yielded accurate data: Larvik in Norway (Norsk Meteornettverk) and Kyyjärvi, Nyrölä, and Tampere (Finnish Fireball Network). None of the stations could observe the terminal point of the fireball due to the large distances and the low terminal height of the fireball.

Table 1
Characteristic Values of the Triangulated Fireball Trajectory

Parameter	Beginning	End[a]
Latitude [deg]	59.74	59.82
Longitude [deg]	16.51	16.84
Height [km]	81.53	11.28

Note.
[a] The end values correspond to the last observable point of the fireball where the height is higher than the actual terminal height of luminous flight. The entry velocity was determined as 17.52 km s^{-1}.

Table 2
Orbital Elements of the Meteoroid Obtained Using the FireOwl Software for the Epoch JD 2459160.5 (2020 November 7)

Orbital Element	Value	Error
Semimajor axis a *[au]*	**1.90**	**0.025**
Eccentricity e	**0.53**	**0.006**
Inclination i *[deg]*	**15.22**	**0.14**
Longitude of the ascending node Ω [deg]	**226.189**	**0.0004**
Perihelion argument ω *[deg]*	**223.91**	**0.5**
Mean anomaly M *[deg]*	**347.72**	0.5

If the origin of the meteoroid is sufficiently recent, then we can expect a close affinity between the orbits of the meteoroid and its parent body, and thus a small distance between their orbital elements. Given this, we used the metrics proposed by Nesvorný & Vokrouhlický (2006) to calculate the distance d between the two bodies in the space of osculating orbital elements. The smaller the distance, the more akin the corresponding osculating orbits.

The distance d between the orbital elements is defined by the following metrics (Nesvorný & Vokrouhlický 2006):

$$\left(\frac{d}{na}\right)^2 = k_{\rm a}\left(\frac{\delta a}{a}\right)^2 + k_{\rm e}(\delta e)^2 + k_{\rm i}(\delta \sin i)^2 + k_{\Omega}(\delta\Omega)^2 + k_{\varpi}(\delta\varpi)^2. \quad (2)$$

Here, a is the semimajor axis, e is the eccentricity, i is the inclination, Ω is the longitude of the ascending node, ϖ is the longitude of perihelion, δ denotes the differences between the Keplerian elements of the considered orbits, and n is the mean motion of the asteroid. The coefficients in the metrics are chosen according to Nesvorný & Vokrouhlický (2006): $k_a = 5/4$, $k_e = k_i = 2$, $k_\Omega = k_\varpi = 10^{-4}$.

We used both the Tisserand parameter $T_{\rm E}$ and the distance between orbital elements d to pre-select the neighboring bodies as the candidates of possible parent bodies. The Tisserand parameter is expected to be better conserved but has a higher probability of coinciding by chance, whereas the distance between orbital elements is more susceptible to perturbations. In our survey, we constrained ourselves to the closest neighbors because asteroids situated further away are less likely to yield close encounters. Still, there is the possibility that the parent

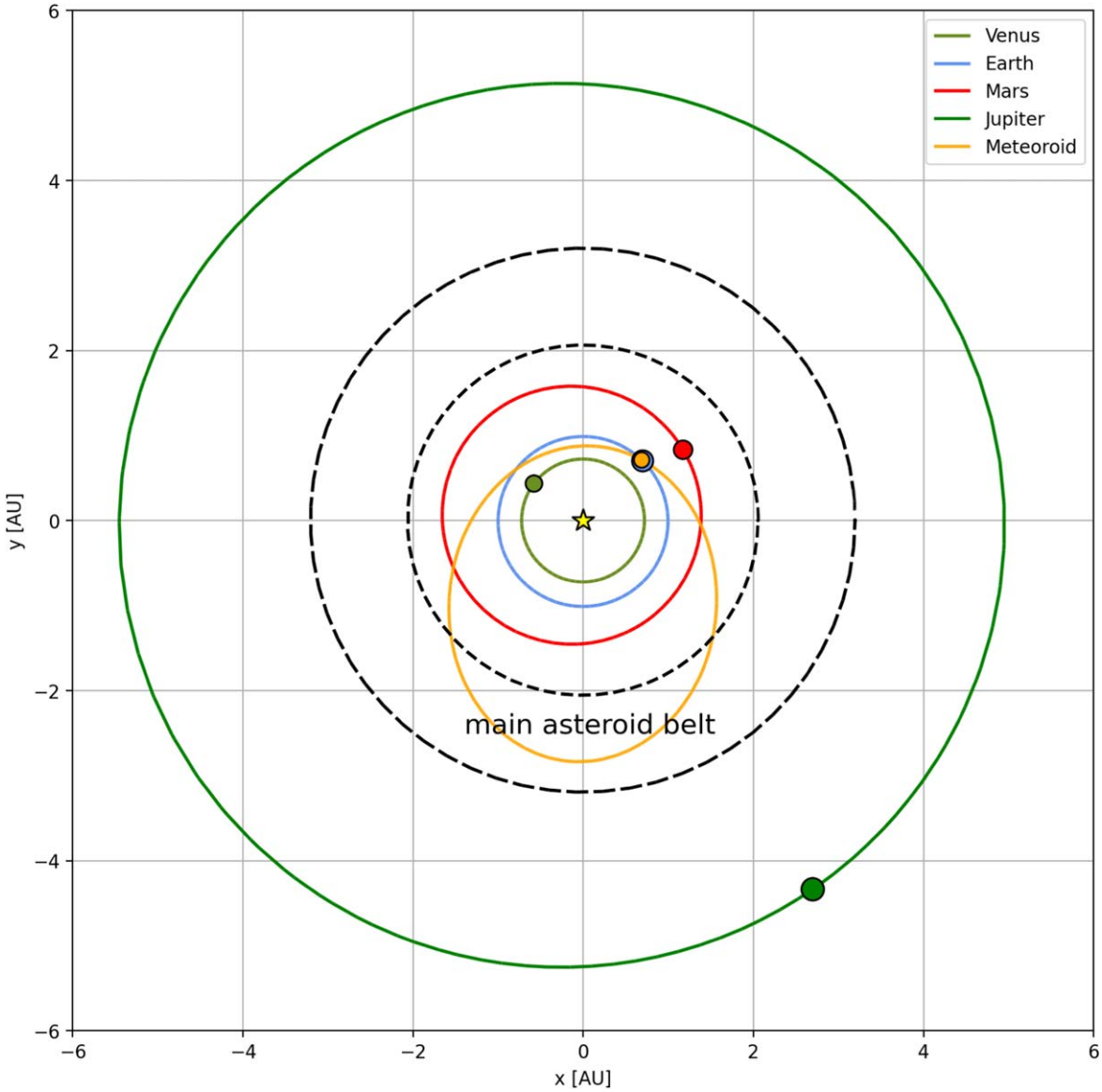

Figure 2. Visual representation of the meteoroid's orbit for the epoch JD 2459160.5 in the inner region of the main asteroid belt (black).

body has orbital parameters very different from those of the meteoroid because its orbit changed due to a very unlikely occasion of a gravitational perturbation of a large magnitude. The distance between orbital elements d and the Tisserand parameter $T_{\rm E}$ of the closest neighbors of the meteoroid are shown in Figure 4.

As a frame for computations, we built a model consisting of all the solar system planets and the most massive bodies of the main belt, which are Ceres, Vesta, and Pallas. Besides planets, these bodies are the principal main-belt perturbers and can significantly influence the behavior of asteroids (e.g., Galád 2012). The general relativity corrections have also been taken into account. Planets with moons, except Earth, are represented by their barycenters. Considering that we aim to model near-Earth asteroids, which could have close encounters with the Earth, the Moon–Earth system is present as separate bodies.

The orbital parameters of parent body candidates and the covariance matrices of their uncertainties are taken from the JPL Horizons system, and clones representing them in the simulations were generated using the same algorithm as in Kyrylenko et al. (2021). The simulations take into account the Yarkovsky effect implemented in GENGA by utilizing the scheme of Vokrouhlický et al. (2000), which modifies the state of an asteroid via a corresponding velocity kick.

The initial selection process resulted in 35 suitable candidates (Figure 4), every one of which was represented by 500 test particles in the modeling. The meteoroid was represented by 10,000 clones, resulting in 5×10^6 unique pairs for each asteroid candidate effectively. They were numerically integrated backward in time recording relative distances and velocities between the candidate and the meteoroid clones in the Cartesian space. The encounters between particles were traced and recorded via a built-in "report encounters" feature based on the Bounding Volume Hierarchy (BVH) method. To detect high-velocity encounters inherent to the separation of collisional nature, the simulations were carried out with a base time step of 12 hr and eight recursion sub-steps for the integrator, which should allow us to detect close encounters of meteoroid with a parent body within 1000 km distance at 1–5 km s^{-1} of relative velocity (Bottke et al. 2015).

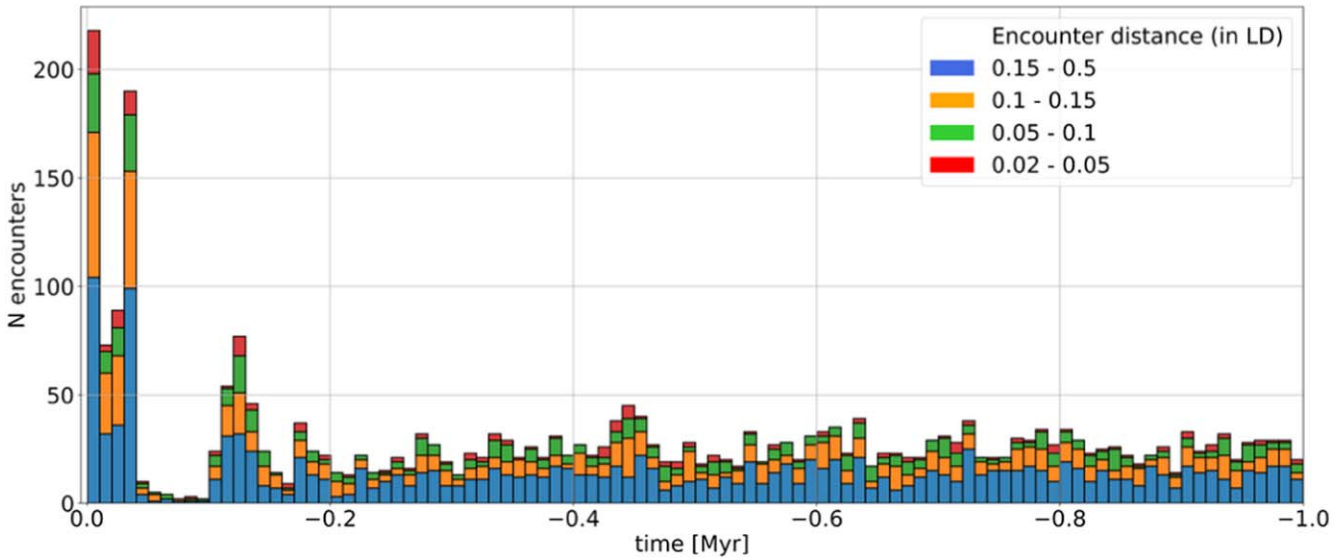

Figure 3. Distribution of clones of the meteoroid over minimal distance with the Earth. The different colors show the range of encounter distances (given in units of Lunar distances LD), stacked on top of each other.

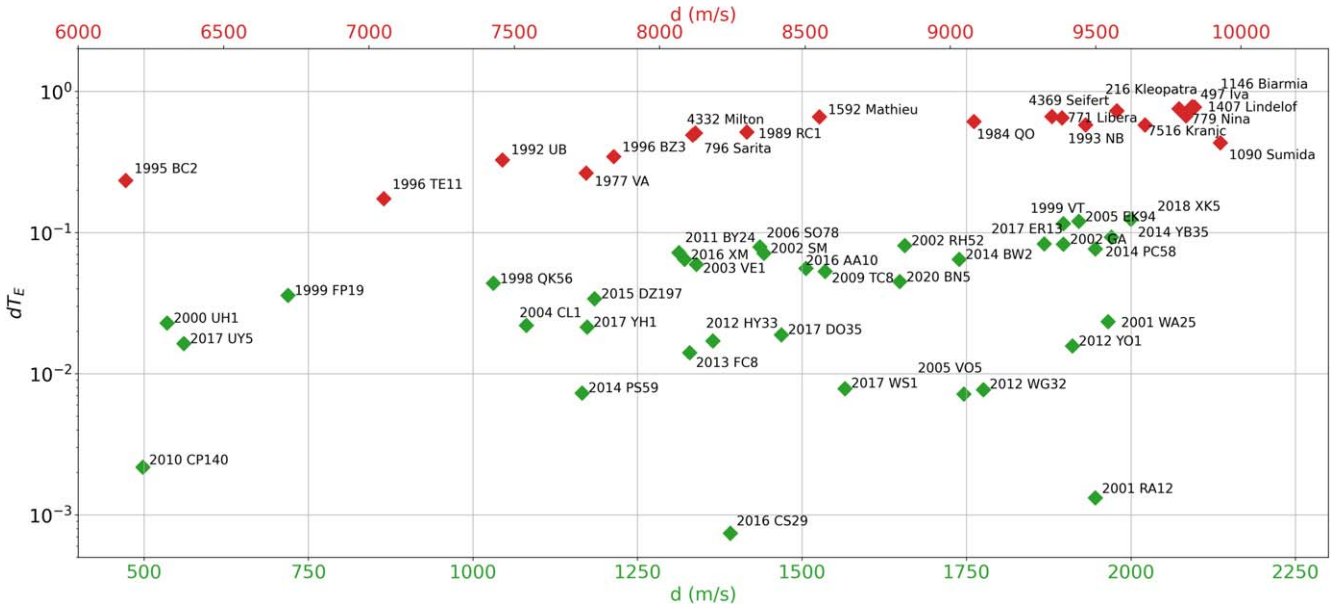

Figure 4. Difference of five-dimensional distance vs. Tisserand parameter for the meteoroid and the neighboring asteroids (marked green, most of them have not been classified yet) and known or suspected M-type asteroids (marked red).

The results of integration show no distinctive candidate into a parent body at the time span of 1 million years because no orbits with acceptably close encounters were traced (Figure 5). This result might indicate that the real parent body lies beyond this time limit or is not present among selected asteroids. The fact that most candidates have high and comparable relative velocities together with distances at the time of their closest approach supports this conclusion. We also attempted to search for close encounters between the meteoroid and known or suspected M-type asteroids. Some M-type asteroids are expected to be iron composition and could potentially be parent bodies of such iron meteoroids. In total, 21 candidates were selected and checked, none of which showed any significant encounter (Figure 5).

2.4. YORP Lifetime Estimate

Let us estimate whether the meteoroid could have survived sufficiently long enough to travel from the main asteroid belt to its near-Earth orbit without being disintegrated. The major grinding mechanism for small meteoroids is the YORP effect: asymmetric scattering and re-emission of the solar radiation exerts torque, which speeds up the meteoroid's rotation until it gets disrupted by centrifugal forces.

The torque exerted upon the meteoroid by the YORP effect can be computed as (Golubov et al. 2016; Marzari et al. 2020)

$$T = \frac{\Phi C r^3}{c a^2 \sqrt{1 - e^2}}. \quad (3)$$

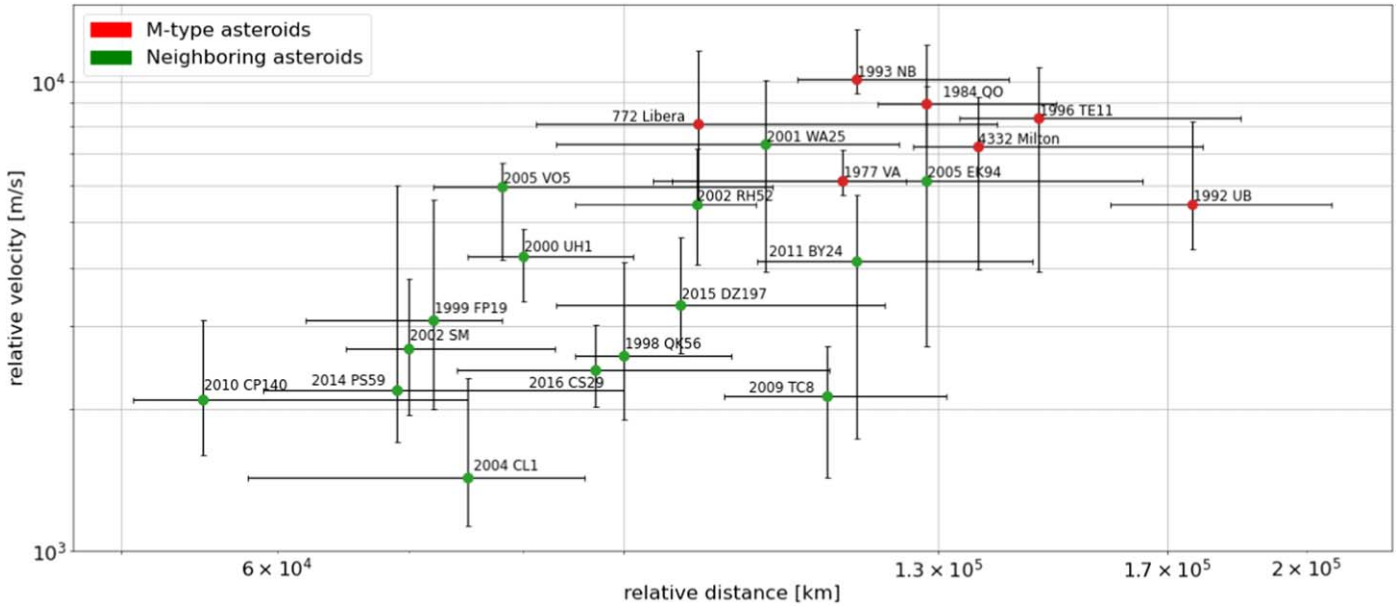

Figure 5. Encounter distances and velocities of neighboring and known or suspected M-type asteroids relative to the clones of the meteoroid in numerical integration up to 1 Myr backward in time. Errorbars represent 5th and 95th percentiles of values, only asteroids with a number of encounters $n \geqslant 10$ are shown.

Here, $\Phi = 1361\ \mathrm{W\,m^{-2}}$ is the solar constant at 1 au, a is the semimajor axis expressed in au, e is the eccentricity, c is the speed of light, r is the radius of the meteoroid, and C is the dimensionless YORP coefficient. The YORP coefficient lies in the range of 0.002–0.02 for most asteroid shapes (Marzari et al. 2020), and we can expect the meteoroid to have it within the same order of magnitude.

This torque causes the meteoroid to experience the angular acceleration $d\omega/dt = T/I$, where I is the moment of inertia. Assuming for the estimate a spherical shape of the meteoroid, we get

$$I = \frac{8}{15}\pi\rho r^5, \tag{4}$$

with ρ being the meteoroid's density.

The disruption limit of a small body held together by a tensile strength σ can be estimated as (Sánchez & Scheeres 2014):

$$\omega \approx \sqrt{\frac{2\sigma}{\rho r^2}}. \tag{5}$$

The measured values of tensile strength for iron meteorites range between 43 and 483 MPa, with the mean value 340 MPa (Pohl & Britt 2020).

Dividing the critical rotation rate by the angular acceleration, we find the YORP timescale of the meteorite:

$$t \approx \frac{8\pi rca^2\sqrt{1-e^2}}{15\Phi C}\sqrt{2\sigma\rho}. \tag{6}$$

We substitute the orbital parameters of the meteorite from Table 2 and assume the meteoroid's size $r \approx 0.75$ m. This results in the YORP lifetime estimate in the range $2\ \mathrm{Myr} \lesssim t \lesssim 20\ \mathrm{Myr}$.

As the YORP lifetime estimate suggests, the meteoroid could have survived long enough to transit the resonance independently to enter the near-Earth region. Since the dynamics within the resonance are highly chaotic, crossing the resonance effectively erases the information about the initial orbit and leaves no chance of recovering the parent body by standard means.

2.5. Source Region of the Meteoroid in the Main Belt

Regardless of whether the meteoroid originated in situ in the near-Earth region or survived its travel from the main belt, the analysis of its orbit allows us to determine the source region of the meteoroid or its parent body. Using the NEOPOP software (Granvik & Brown 2018), which implements the debiased distribution model of the asteroids in the near-Earth region, we estimated the statistical possibility of source regions of the meteoroid based on its derived orbit. The results shown in Table 3 indicate that the ν_6 secular resonance with Saturn and the 3:1 mean-motion resonance with Jupiter are by far the most probable sources of the meteoroid.

Figure 6 illustrates the distribution of semimajor axis a, eccentricity e, and the inclination of i of the meteoroid's clones which were generated within the uncertainties and propagated 1 Myr backward in time. The uncertainties of the initial conditions cause heavy spreading of the clones' orbital elements and limit the possible propagation time for credible modeling. The distribution of the semimajor axis clearly shows that clones tend to group close to 1.9 and 2.1 au, which corresponds to the boundaries of ν_6 secular resonance. The results are roughly consistent with those obtained via the NEOPOP software and confirm the ν_6 resonance as the most plausible source region of the meteoroid.

3. Discussion

The reconstructed orbit of the iron meteoroid lies in an unstable region close to the ν_6 secular resonance with Saturn and the 3:1 mean-motion resonance (MMR) with Jupiter. The results of the statistical modeling and numerical approach also converge to the conclusion that either ν_6 or J3:1 (MMR) is the escape route of the meteoroid. These two resonances are responsible for the delivery of most of the near-Earth asteroids from the main belt (Bottke et al. 2002; Granvik & Brown 2018). The area bordering these resonances includes a large

Table 3
Probability of the Most Plausible Source Regions for the Iron Meteorite Computed with the NEOPOP Software

Source Regions	Probability (%)
ν_6 secular resonance	89
J3:1 mean-motion resonance	10
J5:2 mean-motion resonance	<1

number of weaker mean-motion resonances with Earth, Mars, and Venus (Gallardo 2006), which can facilitate the migration of the meteoroid's orbit toward one of the stronger resonances.

The adjacent part of the inner main belt hosts the largest asteroid families Vesta, Flora, and the Nysa-Polyana complex (Nesvorný 2015). It was estimated that 85% of the asteroids in the inner region of the main belt could come from the aforementioned largest families (Dermott et al. 2018). Although Vesta is a differentiated body with a metallic core (Russell et al. 2012), its family is of mostly silicate composition because the family producing collision was not sufficiently energetic to affect Vesta's core. Nevertheless, Vesta and Nysa-Polyana families are known to contain some identified M-type asteroids. The Baptistina family, which is also situated in the inner main belt, is dominated by the M-type asteroids (Slyusarev & Shymkiv 2017; Slyusarev 2018). Still, all these families have small inclinations (2°–7°) in comparison to the meteoroid, making it unlikely for the meteoroid to originate from either of these families. More probably, the meteoroid came from the non-family background of M-type asteroids dispersed in this region of the inner main belt. A dozen M-type asteroids have close values of the inclination (12°–17°) and semimajor axis (2.0–2.5 au) to those of the meteoroid.

The orbit of the iron meteoroid is quite typical if compared to the known orbits of other meteoroids (www.meteoriteorbits.info) and the orbits of asteroids of the Apollo and Amor groups, as can be seen in Figure 7. The orbit of the Sikhote-Alin meteoroid, determined according to the interviews with eyewitnesses, has a close semimajor axis and an eccentricity similar to those of the meteoroid ($a = 2.16$ au; $e = 0.536$), whereas its inclination is almost two times smaller ($i = 9.^{\circ}4$) (Fesenkov 1951). From Figure 7, one can see no clear distinction between the orbits of iron and stony meteoroids.

The results of numerical integrations indicate that none of the tested asteroids satisfy the requirements of a parent body at the time span of 1 million years. This result might indicate that the separation of the meteoroid from its parent body lies beyond this time limit or that the parent body is not present among selected asteroids. The result is acceptable because even well-determined orbital properties (e.g., Almahata Sitta/2008 TC3, Jenniskens et al. 2010) do not guarantee the successful identification of the parent body.

Although we can be quite certain that the material composing the meteoroid arrived from the inner main belt, it leaves open two possibilities for where the meteoroid left its parent body. First, the material of the meteoroid could have exited the main belt as a part of a larger near-Earth asteroid and recently split from it. Second, the meteoroid could have split from the parent body in the main belt and was delivered to a near-earth orbit already in its present form. In either case, the meteoroid could not have existed as a separate body for too long because such small bodies have a limited lifetime, they permanently get disrupted, and their population is resupplied via the decay of larger bodies.

The split of a meteoroid from a larger body could have occurred either due to a collision of the parent body with another asteroid or due to the supercritical rotation of the parent body and its destruction by centrifugal forces. The required supercritical rotation can be produced by the YORP effect, i.e., the radiation pressure torque caused by the asymmetric scattering and emission of radiation by the asteroid (e.g., Vokrouhlický et al. 2015). Both YORP and collisions can significantly contribute to the grinding of small main-belt asteroids into smaller chunks, whereas YORP is the only dominant mechanism that can grind near-Earth asteroids because the near-Earth region is very scarcely populated by asteroids, which makes the collisions much less frequent. The meteoroid, created as a result of such decay, is subject to the same two grinding processes, which limit its lifetime and determine how far its orbit can evolve. The estimated size of the meteoroid is about 1 m.[11] For such small objects, YORP is the dominant disaggregation process, even in the main belt, and increases for the near-Earth asteroids. Still, iron meteorites are known to have high tensile strength (Pohl & Britt 2020), which makes it easier for them to withstand large centrifugal forces and enlarges the time necessary for the meteoroid to be disaggregated by the YORP effect. We find the disaggregation time of the meteoroid to be of the order of 10 Myr. This lifetime is longer than the typical time for non-metallic bodies of the same size, giving the meteoroid enough time to start from the main belt and reach its current orbit. This YORP timescale is also of the same order of magnitude as the typical lifetimes of asteroids and meteoroids on near-Earth orbits, which are at the order of 10 Myr (Bottke et al. 2002; Granvik & Brown 2018).

Essential information about the history of the meteoroid can be obtained from the CRE time. This dating method measures the abundance of cosmogenic nuclides in a sample and allows the period during which the sample was exposed to cosmic rays to be computed. In the case of the meteoroid, this corresponds to the time span after the separation from the parent body and before the atmospheric entry. We do not expect the meteoroid to be younger than 1 Myr because no parent body was found in numerical simulations within this limit. Meanwhile, the YORP lifetime of the meteoroid from our estimates is at most about 20 Myr, which sets an upper boundary on its age. Therefore, we anticipate that the CRE age of the meteorite should be in the range of 1–20 Myr. Subsequent laboratory analysis of the meteorite might provide information about its CRE age and can test our idea of the meteoroid surviving a long travel from the inner part of the main asteroid belt to the near-Earth orbit without being disintegrated.

4. Conclusions

The first instrumentally documented fall of an iron meteorite gave us a unique opportunity to investigate the reservoir of metallic asteroids in the solar system. Available observations of the fireball allowed us to compute its pre-atmospheric orbit. The reconstructed orbit of the iron meteorite shows no distinctive features in comparison with the previously recorded falls of stony meteorites and is typical for near-Earth asteroids. The statistical model suggests ν_6 secular resonance with Saturn (89%) and 3:1 mean-motion resonance with Jupiter (10%) to be

[11] International Meteor Organization, https://www.imo.net/swedish-nov-7-fireball-as-bright-as-full-moon/.

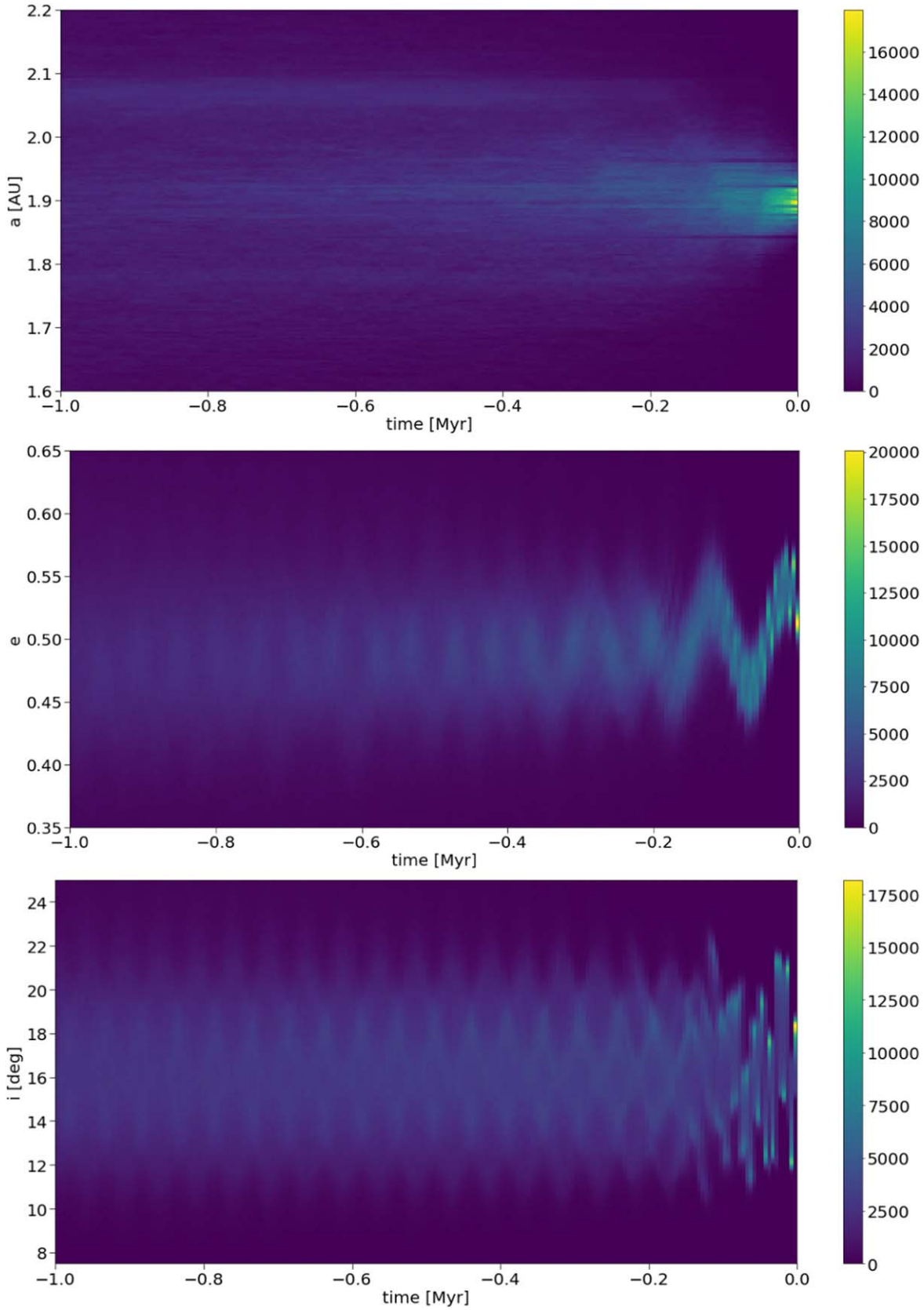

Figure 6. Distribution of the *a*, *e*, *i* orbital elements of meteoroid clones in numerical integration up to 1 million years backward in time.

the primary candidates for the escape routes of the meteoroid, which also are the main suppliers of other near-Earth asteroids in the main asteroid belt. The results of backward numerical integrations indicate that the meteoroid probably left its parent body no later than 1 Myr ago, while the complex evolutionary dynamics in the vicinity of Earth and the ν_6 and J3:1

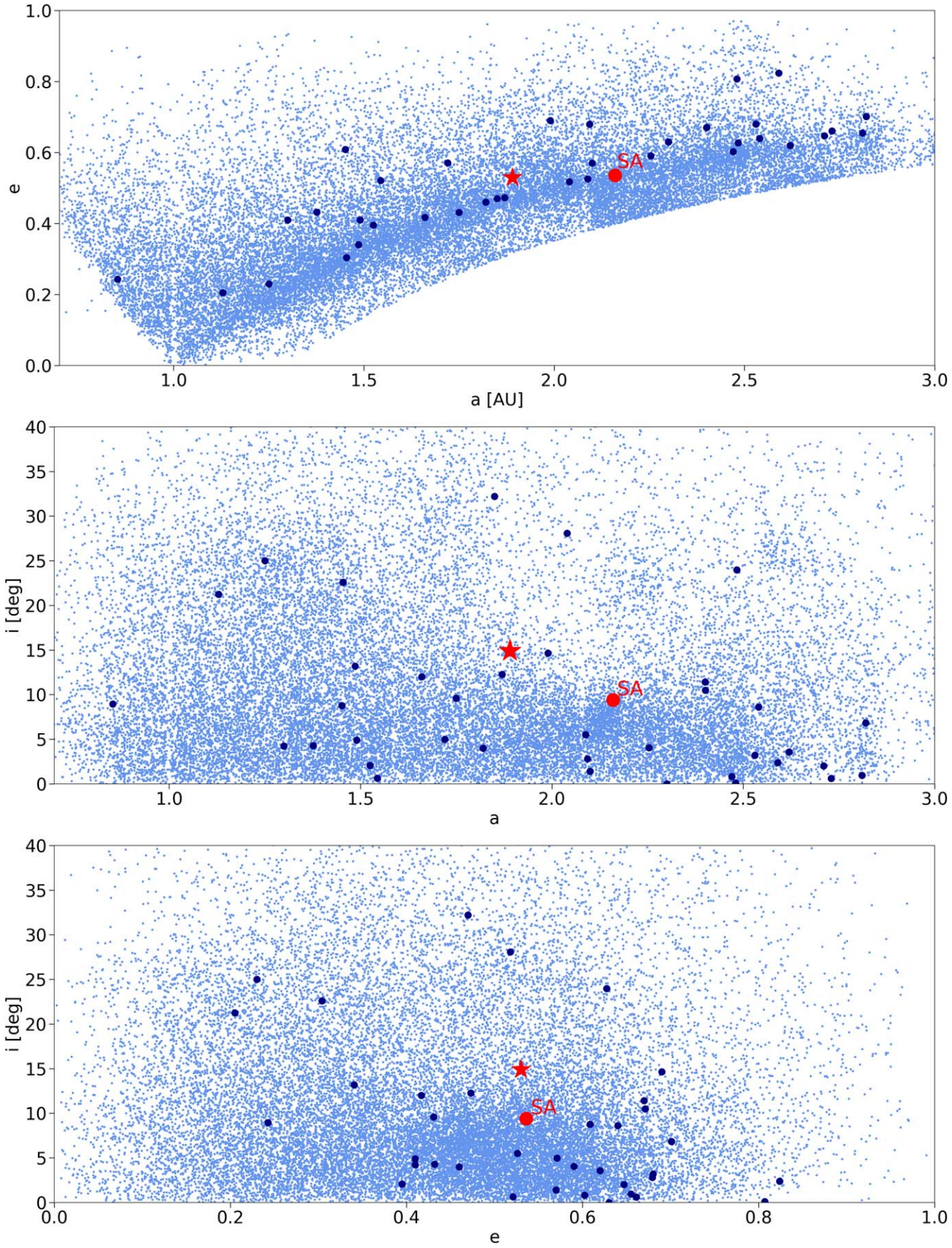

Figure 7. Comparison of the orbital elements of the iron meteoroid (red star symbol) with the orbits of near-Earth asteroids (sky-blue) and the above-mentioned meteoroids with known heliocentric orbits (blue). The highly uncertain orbital elements of Sikhote-Alin (Fesenkov 1951) are also shown (red circle).

resonances aggravate the reliable identification of a parent body beyond this time limit. The YORP timescale of the meteoroid is estimated to be about 20 Myr. This timescale is sufficiently long for the meteoroid to survive the journey from the main asteroid belt to a near-Earth orbit. The long YORP timescale supports the numerical results on the absence of close passages between the meteoroid and selected near-Earth asteroids. The meteoroid which fell near the village of Ådalen supersedes the Sikhote-Alin as the iron meteoroid with the most accurately determined orbit. The rapid development of automatic meteor networks gives us hope for the registration of more falls of iron meteorites in the next few years, which could give us more information about their sources in the solar system.

Acknowledgments

The work of the Ukrainian team was funded by the National Research Foundation of Ukraine, project N2020.02/0371 "Metallic asteroids: search for parent bodies of iron meteorites, sources of extraterrestrial resources." M.G. acknowledges the Academy of Finland project no. 325806 (PlanetS). We thank all members of the Finnish Fireball Network, especially Esko Lyytinen and Jarmo Moilanen, for their dedicated commitment, and acknowledge Ursa Astronomical Association for the support with the Network coordination. We are grateful to all the other scientists and observers across the Nordic region who contributed to the discussions and acquisition of the data, as well as to geologists Andreas Forsberg and Anders Zetterqvist who reported the meteorite find, and to Johan Benzelstierna von Engeström for his enthusiasm and overall support of the meteorite searches in the area. The authors thank the reviewer of this article for their insightful suggestions, which led to a significant improvement of this article. I.B. thanks the support of the PAUSE program for scientists in danger. O.G. and Y. K. thank the support of the ALLEA and the Breakthrough Prize Foundation for scientists impacted by the war in Ukraine, projects ALLEA EFDS-FL1-16 and ALLEA EFDS-FL1-18.

Data Availability

The data underlying this article will be shared on a reasonable request to the corresponding author.

ORCID iDs

Ihor Kyrylenko https://orcid.org/0000-0002-9326-4544
Oleksiy Golubov https://orcid.org/0000-0002-2427-9101
Ivan Slyusarev https://orcid.org/0000-0003-4919-8225
Maria Gritsevich https://orcid.org/0000-0003-4268-6277
Yurij N. Krugly https://orcid.org/0000-0002-3171-9873
Irina Belskaya https://orcid.org/0000-0002-5796-6493
Vasilij G. Shevchenko https://orcid.org/0000-0003-1000-223X

References

Andrade, M., Docobo, J. Ã., García-Guinea, J., et al. 2022, MNRAS, 518, 3850
Astapovich, I. S. 1939, AZh, 16, 15
Boaca, I., Gritsevich, M., Birlan, M., et al. 2022, ApJ, 936, 150
Borovička, J., Spurný, P., Brown, P., et al. 2013, Natur, 503, 235
Bottke, W. F., Broz, M., O'Brien, D. P., et al. 2015, in Asteroids IV, ed. M Patrick , F. E. DeMeo, & W. F. Bottke, Vol. 1 (Tucson, AZ: Univ. Arizona Press), 701
Bottke, W. F., Morbidelli, A., Jedicke, R., et al. 2002, Icar, 156, 399
Bottke, W. F., Nesvorný, D., Grimm, R. E., Morbidelli, A., & O'Brien, D. P. 2006, Natur, 439, 821
Burbine, T. H., McCoy, T. J., Meibom, A., Gladman, B., & Keil, K. 2002, in Asteroids III, ed. W. F. Bottke, A. Cellino, P. Paolicchi, & R. P. Binzel (Tucson, AZ: Univ. Arizona Press), 653
Colas, F., Zanda, B., Bouley, S., et al. 2020, A&A, 644, A53
de La Fuente Marcos, C., & de La Fuente Marcos, R. 2014, MNRAS Lett., 443, L39
Dermott, S. F., Christou, A. A., Li, D., Kehoe, T. J., & Robinson, J. M. 2018, NatAs, 2, 549
Dmitriev, V., Lupovka, V., & Gritsevich, M. 2015, P&SS, 117, 223
Dmitriev, V., Lupovka, V., & Gritsevich, M. 2018, M&PS, 53, 6210
Fesenkov, V. G. 1951, Metik, 9, 27
Galád, A. 2012, A&A, 548, A25
Gallardo, T. 2006, Icar, 184, 29
Gardiol, D., Barghini, D., Buzzoni, A., et al. 2021, MNRAS, 501, 1215
Goldstein, J., Scott, E., & Chabot, N. 2009, Geoch, 69, 293
Golubov, O., Kravets, Y., Krugly, Y. N., & Scheeres, D. 2016, MNRAS, 458, 3977
Granvik, M., & Brown, P. 2018, Icar, 311, 271
Grimm, S. L., & Stadel, J. G. 2014, ApJ, 796, 23
Gritsevich, M. I, 2009, AdSpR, 44, 323
Gritsevich, M., Dmitriev, V., Vinnikov, V., et al. 2017, in Assessment and Mitigation of Asteroid Impact Hazards, ed. J. Trigo-Rodríguez, M. Gritsevich, & H. Palme (Cham: Springer), 153
Gritsevich, M., Nissinen, M., Moilanen, J., et al. 2021, JIMO, 49, 52
Gritsevich, M. I., Stulov, V. P., & Turchak, L. I, 2012, CosRe, 50, 56
Jenniskens, P. 2004, AJ, 127, 3018
Jenniskens, P., Vaubaillon, J., Binzel, R. P., et al. 2010, M&PS, 45, 1590
Kaminski, E., Limare, A., Kenda, B., & Chaussidon, M. 2020, E&PSL, 548, 116469
King, A. J., Daly, L., Rowe, J., et al. 2022, SciA, 8, eabq3925
Kyrylenko, I., Krugly, Y. N., & Golubov, O. 2021, A&A, 655, A14
Lyytinen, E., & Gritsevich, M. 2013, in Proc. Int. Meteor Conf., ed. M. Gyssens & P. Roggemans (Hove: International Meteor Organization), 155
Lyytinen, E., & Gritsevich, M. 2016a, in Proc. Int. Meteor Conf., ed. A. Roggemans & P. Roggemans (Hove: International Meteor Organization), 159
Lyytinen, E., & Gritsevich, M. 2016b, P&SS, 120, 35
Marzari, F., Rossi, A., Golubov, O., & Scheeres, D. J. 2020, AJ, 160, 128
Moilanen, J., & Gritsevich, M. 2021, LPICo, 2609, 6252
Moilanen, J., & Gritsevich, M. 2022, LPICo, 2678, 2933
Moilanen, J., Gritsevich, M., & Lyytinen, E. 2021, MNRAS, 503, 3337
Moreno-Ibáñez, M., Gritsevich, M., Trigo-Rodríguez, J. M., & Silber, E. A. 2020, MNRAS, 494, 316
Murray, C. D., & Dermott, S. F. 1999, Solar System Dynamics (Cambridge: Cambridge Univ. Press), 72
Nesvorný, D. 2006, Nesvorný HCM Asteroid Families V3.0, 132, 1950, https://pds.nasa.gov/ds-view/pds/viewDataset.jsp?dsid=EAR-A-VARGBDET-5-NESVORNYFAM-V3.0
Nesvorný, D., & Vokrouhlický, D. 2006, AJ, 132, 1950
Peña-Asensio, E., Trigo-Rodríguez, J. M., Gritsevich, M., & Rimola, A. 2021, MNRAS, 504, 4829
Peña-Asensio, E., Trigo-Rodríguez, J. M., Rimola, A., Corretgẽ-Gilart, M., & Koschny, D. 2023, MNRAS, 520, 5173
Pickering, W. H. 1910, PA, 18, 262
Pohl, L., & Britt, D. T. 2020, M&PS, 55, 962
Russell, C., Raymond, C., Coradini, A., et al. 2012, Sci, 336, 684
Sánchez, P., & Scheeres, D. J. 2014, M&PS, 49, 788
Sansom, E. K., Gritsevich, M., Devillepoix, H. A., et al. 2019, ApJ, 885, 115
Schiaparelli, G. V. 1867, Note E riflessioni intorno alla teoria astronomica delle stelle cadenti (Florence: Stamperia Reale)
Scott, E. R. D. 2020, Iron Meteorites: Composition, Age, and Origin (Oxford: Oxford Univ. Press)
Shrbený, L., Krzesińska, A. M., Borovička, J., et al. 2022, M&PS, 57, 2108
Slyusarev, I., & Shymkiv, D. 2017, in European Planetary Science Congress 2017 (Göttingen: Copernicus), 909
Slyusarev, I. G. 2018, in Proc. IAU 14, Astronomy in Focus XXX, ed. M. Teresa Lago (Cambridge: Cambridge Univ. Press), 21
Trigo-Rodríguez, J. M., Lyytinen, E., Gritsevich, M., et al. 2015, MNRAS, 449, 2119
Visuri, J., & Gritsevich, M. 2021, LPICo, 2609, 6093
Vokrouhlický, D., Bottke, W. F., Chesley, S. R., et al. 2015, in Asteroids IV, ed. Patrick Michel, F. E. DeMeo, & W. F. Bottke (Tucson, AZ: Univ. Arizona Press), 509
Vokrouhlický, D., Milani, A., Chesley, S., et al. 2000, Icar, 148, 118
Whipple, F. L. 1983, IAUC, 3881, 1